

Regular paper

Outage Probability of NOMA System with Wireless Power Transfer at Source and Full-Duplex Relay

Ba Cao Nguyen, Tran Manh Hoang, Phuong T. Tran, Tan N. Nguyen

PII: S1434-8411(19)31414-1
DOI: <https://doi.org/10.1016/j.aeue.2019.152957>
Reference: AEUE 152957

To appear in: *International Journal of Electronics and Communications*

Received Date: 4 June 2019
Accepted Date: 11 October 2019

Please cite this article as: B.C. Nguyen, T.M. Hoang, P.T. Tran, T.N. Nguyen, Outage Probability of NOMA System with Wireless Power Transfer at Source and Full-Duplex Relay, *International Journal of Electronics and Communications* (2019), doi: <https://doi.org/10.1016/j.aeue.2019.152957>

This is a PDF file of an article that has undergone enhancements after acceptance, such as the addition of a cover page and metadata, and formatting for readability, but it is not yet the definitive version of record. This version will undergo additional copyediting, typesetting and review before it is published in its final form, but we are providing this version to give early visibility of the article. Please note that, during the production process, errors may be discovered which could affect the content, and all legal disclaimers that apply to the journal pertain.

© 2019 Published by Elsevier GmbH.



Outage Probability of NOMA System with Wireless Power Transfer at Source and Full-Duplex Relay

Ba Cao Nguyen^a, Tran Manh Hoang^a, Phuong T. Tran^{b,1,*}, Tan N. Nguyen^b

^a*Faculty of Radio Electronics, Le Quy Don Technical University, Vietnam*

^b*Wireless Communications Research Group, Faculty of Electrical and Electronics Engineering, Ton Duc Thang University, Ho Chi Minh City, Vietnam*

Abstract

In this paper, we analyze the performance of a novel communication scheme that combines three new techniques, namely energy harvesting (EH), full-duplex (FD) relay and cooperative non-orthogonal multiple access (NOMA). In this scheme, both the source and the relay harvest energy from the power beacon (PB) at the first phase of the transmission block and then use the harvested energy to transmit messages during the remaining phase. In this proposed EH-FD-NOMA system, the FD relay employs the amplify-and-forward scheme. We consider two destinations, one of them is far from the FD relay and the other is near the FD relay. Based on the mathematical calculation, we derive the closed-form expressions for the outage probability (OP) of the two users of interest. The numerical results show that the performance at two destinations can be maintained at the same level with proper power allocation. Furthermore, for each value of the PB transmit power, there exists an optimal value for the EH time duration to improve the performance of both users. In addition, the impact of the residual self-interference (RSI) due to imperfect self-interference cancellation (SIC) at the FD relay is also considered. Finally, numerical results are demonstrated through Monte-Carlo simulations.

Keywords: Energy harvesting, in-band full-duplex relay, self-interference (SI), self-interference cancellation (SIC), amplify-and-forward, NOMA, successive interference cancellation, outage probability.

1. Introduction

In the digital era today, the wireless devices are continuously upgraded on the hardware, software, and firmware to adapt to the development of the world. With the growth of data exchange demand, especially for the Internet of Things (IoT) devices and the future wireless networks, i.e. the fifth generation (5G) of mobile communications, many studies to improve the spectrum efficiency of wireless

*Corresponding author, Ton Duc Thang University, Ho Chi Minh City, Vietnam

Email addresses: bacao.sqtt@gmail.com (Ba Cao Nguyen), tranmanhhoang@tcu.edu.vn (Tran Manh Hoang), tranthanhphuong@tdtu.edu.vn (Phuong T. Tran), nguyennhattan@tdtu.edu.vn (Tan N. Nguyen)

¹Address: Ton Duc Thang University, No. 19 Nguyen Huu Tho Street, Tan Phong Ward, District 7, Ho Chi Minh City, Vietnam

systems have been proposed, such as massive multiple-input multiple-output (MIMO), non-orthogonal multiple access (NOMA), full-duplex (FD) or in-band full-duplex (IBFD). Based on these ideas, a lot of research and experiments have also been conducted to implement them on practical systems [1, 2, 3]. In the ideal case, the FD communication has potential to double the system capacity due to its allowance to transmit and receive the signals simultaneously within the same frequency band [2, 3, 4, 5, 6, 7]. In the indoor scenarios, the FD communication has been proved to improve from 30 to 40% of capacity, compared with the half-duplex (HD) communication [2, 8]. Therefore, the FD communication is a promising technique for many applications, such as 5G, cognitive radio networks, device-to-device communications, small cells [2, 3, 9]. Besides the FD, the NOMA technology has also attracted a lot of attention in recent years due to the fact that it can share the same time, frequency, and code resources among all users [10, 11, 12, 13, 14]. Thus, it can improve the down-link performance, and provide higher spectrum efficiency than the traditional orthogonal multiple access method (OMA). The combination of FD and NOMA techniques becomes a promising technology for the future wireless networks [11, 12].

On the other hand, the wireless energy transfer has been an inevitable trend in recent years due to its undoubtful benefits. It led to the studies of the energy harvesting (EH) from the surrounding environment to provide a continuous energy supply for wireless networks [15, 16, 17]. Wherein, the EH from radio frequency (RF) at the relay nodes in the wireless relay networks has been analyzed rigorously, such as [15, 16, 17, 18, 19, 20]. In the literature, the relay node has the limited power supply; thus it firstly harvests the energy from the source node or power beacon (PB), then converts the collected energy to the power supply for the signal transmitting and receiving [15, 16, 17, 18, 19, 20]. Furthermore, through both experiment and modeling, the results in [21] and [22] demonstrated that the harvested energy can supply enough power for suitable applications, such as for biomedical and sensor devices. Although the nonlinear energy harvesters can operate in wider frequency range, which benefits for energy harvesting from frequency broadband vibrations [23, 24], however, the usage linear energy harvester was suitable for wireless system due to the fact that a linear energy harvester can be tuned to a specific frequency and can efficiently harvest power at their resonance frequency [25].

To extend the coverage and improve the reliability of the wireless systems, the use of the relays that operate in the FD mode is a feasible solution due to the fact that it can be easily deployed with low-cost. As a result, many studies have focused on the performance analysis of the FD relay systems in terms of the outage probability (OP), bit error rate (BER) and ergodic capacity, such as [12, 15, 26, 27, 28]. These above results have demonstrated that the FD systems have the better capacity than the HD systems as long as the residual self-interference (RSI) is below a threshold after using self-interference cancellation (SIC). In other words, the interference cancellation can reduce significantly the OP and BER of the system.

The combination of the FD relaying and NOMA scheme in a single system has been introduced in [16, 11, 29, 30, 31] to improve the spectrum capacity. When the relay is located at an inconvenient place, where the power supply is hard to deploy, it must harvest the energy through RF signals for exchanging the information. In [16], the performance of EH in the NOMA system was investigated. Herein, a strong user harvested the energy from the base station (BS). Then, it can help receive the signal from the BS and simultaneously forward this signal to a weak user in FD mode. In that paper, the strong user employs the decode-and-forward (DF) scheme for FD relaying. In [30], the down-link NOMA system has been analyzed. The authors considered an EH-based relay node that operated in FD mode using the DF scheme. The OPs at both users over Nakagami- m fading channel have been derived in that paper. Furthermore, the optimal value of the time duration has been achieved to maximize the throughput of the system. In 2008, Deng et al. [31] investigated a multiple-input single-output (MISO) NOMA system with FD relay and EH. The optimal transmit power of the dedicated energy transmitter was proposed to improve the system performance.

Although the EH, FD and NOMA techniques are all promising solutions for wireless networks, the studying of the combination of these techniques is still limited, especially when the source and the relay nodes are located at some inconvenient locations. In literature, such as [32, 33, 34, 35], the energy harvesting at source and relay was investigated, however, there are not any studies considering that for NOMA system. One of the reason is due to the computational complexity to derive the performance formulas. Motivated by this fact, in this paper, we propose a combined EH-FD-NOMA system, where both source and relay nodes harvest the energy from a PB, and then exchange the signals. The source node operates in the HD mode while the relay is in FD mode with amplify-and-forward (AF) protocol. Two users, including a strong-connection one and a weak-connection one, are receiving signals in the HD mode. Through the mathematical analysis, we derive the OP expressions for both users over the Rayleigh fading channel. The contributions of this paper can be summarized as follows:

- We propose a novel system model, where the three above-mentioned techniques are combined. It is also noted that these techniques are combined in the previous works, such as [16], but the authors in [16] only considered the case that the relay node harvests the energy from the source node. In our model, we consider the case that both the source node and the FD relay node harvest the energy from the power beacon through RF signals, then use it for information transmission.
- We derive the exact expression for the outage probabilities at both users in the case of imperfect self-interference cancellation at the FD relay node. From here, the throughput expressions of both users are also derived.

- 75 • We analyze the system performance in terms of the OP and throughput for both users over the Rayleigh fading channel. The results show that both users can obtain the same quality of service with proper power allocation. The OP performance of both users is strongly affected by the RSI in the FD mode. On the other hand, with a fixed transmit power of the PB, there exists an optimal value of the time duration for EH to reach the best performance for both users. All
80 these analytical results are verified by the Monte-Carlo simulations.

The rest of this paper is organized as follows. In Section 2, we propose our system model. Then, Section 3 presents the system performance in terms of the OP. Section 4 provides the numerical results and discussions. Finally, in Section 5, we summarize this paper.

2. System Model

85 In this section, we consider an EH-FD-NOMA system, where the signals are transmitted from the source node (S) to two users (D_1 and D_2) with the helping of a relay node (R) as illustrated in Fig. 1. In this system, we investigate the case that S and R do not have their own power supplies. Thus, they must harvest the energy from the PB via RF signals before transmitting information. Here, each node (S, D_1 or D_2) is equipped with a single antenna, and they all operate in the HD mode.
90 Meanwhile, R has two antennas and operates in the FD mode, so it can transmit and receive the signals simultaneously in the same frequency band. The amplify-and-forward (AF) protocol is used in our model. It is noted that in practical systems, R can use one shared-antenna for transmitting and receiving of signals. To serve both users D_1 and D_2 , the S uses non-orthogonal multiple access (NOMA). The user D_1 is located far from the R while the user D_2 is close to the R. Due to the far
95 distances and deep fading, the direct links between the S and the NOMA destination users, i.e., D_1 and D_2 do not exist. In addition, we assume that the PB is located in a convenient area, where the links from the PB to the S and R are always available.

Together with these above assumptions, a two-stage time switching protocol is used for the system as shown in Fig. 2. The entire transmission block of length T is divided into two stages: the first
100 stage has the duration of αT , and the remaining stage has the length of $(1 - \alpha)T$, where α denotes the time switching ratio, $0 \leq \alpha \leq 1$. During the first stage, the PB supplies the energy for the S and R through RF signals. After that, in the second stage, S and R use the harvested energy to transmit or forward the information signals. In particular, S transmits the signal to R, and simultaneously, R broadcasts the signals (received in the previous block) to both D_1 and D_2 . The power processing and
105 converting at S and R are done completely during the first stage.

During the EH interval of αT , the harvested energy at the S and R, denoted by E_h^S and E_h^R are

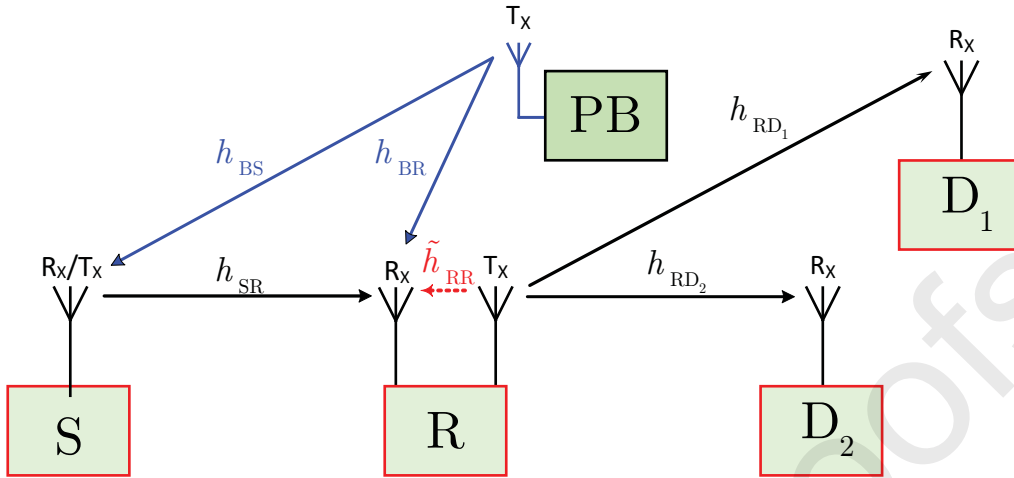


Figure 1: System model of the FD-AF relay system with NOMA and energy harvesting.

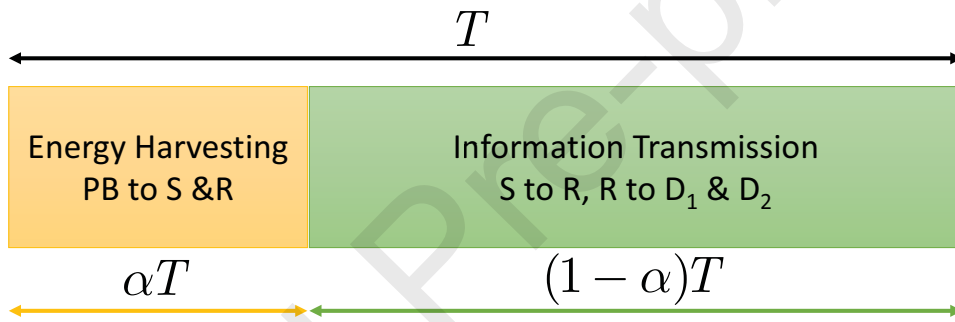


Figure 2: Time switching protocol for energy harvesting at the source and the relay

presented respectively as follows [36]:

$$E_h^S = \eta\alpha TP|h_{BS}|^2, \quad (1)$$

$$E_h^R = \eta\alpha TP|h_{BR}|^2, \quad (2)$$

where P is the average transmit power of the PB; η is the energy conversion efficiency, which depends on the rectification process and the EH circuitry ($0 \leq \eta \leq 1$); h_{BS} , h_{BR} are respectively the fading coefficients of the channels from PB to S and PB to R. It is noted that in this paper we assume that the R only use one antenna for EH. In practical systems, if the R has two antennas, it can use both
 110 antennas to collect energy with suitable hardware resources [37].

We assume that both S and R have super capacitors to store the harvested energy. After the EH stage, the S and R can fully use the harvested energy for transmitting/forwarding the information

during the next interval of $(1 - \alpha)T$. Hence, the transmit power at S and R can be computed as [38]

$$P_S = \frac{\eta\alpha P|h_{BS}|^2}{1 - \alpha} = \frac{\eta\alpha P\rho_1}{1 - \alpha}, \quad (3)$$

$$P_R = \frac{\eta\alpha P|h_{BR}|^2}{1 - \alpha} = \frac{\eta\alpha P\rho_2}{1 - \alpha}, \quad (4)$$

where $\rho_1 = |h_{BS}|^2$, $\rho_2 = |h_{BR}|^2$ are channel gains of the links from PB to S and PB to R, respectively.

During the information transmission stage of the length $(1 - \alpha)T$, the source S transmits the signal to the relay R, which is the combination of the two messages for both destinations D_1 and D_2 using the superposition coding. Simultaneously, the R forwards the received signal from the previous block to both destinations in the same frequency band after amplifying it. The FD mode causes the self-interference at the R. Here, we assume that perfect channel state information (CSI) is available at all nodes in the system. In addition, the feedback links from both users to the relay and from the relay to source node are available, which can help the source to identify the near and far users. By using the mechanism of training pilot sequence [39, 40, 41, 42], the relay R knows the CSI of S – R, and each receiver D_i knows the CSI of the link R – D_i (for $i = 1, 2$). Now, via the feedback channels, each transmitter can get the CSI of its corresponding link. In particular, S gets the CSI of S – R, and R gets the CSI of R – D_i links (for $i = 1, 2$). Finally, because the relay now knows all CSI information of the above-mentioned links, it can send back the necessary information to S (by feedback channel) and $D_i, i = 1, 2$ (by forward channel). As a results, the CSI of all links S – R, R – $D_i, i = 1, 2$ is available at all nodes in the proposed system. These assumptions have been made in many previous works on NOMA systems, such as in [30, 43, 44, 45, 46, 47]. Therefore, the source S can allocate the power for two users properly. Furthermore, we assume that the signal processing delay at the R is equal to one transmission block; thus the signal transmitted from R is the one received from S during the previous block. Therefore, the received signal at R is expressed as

$$y_R = h_{SR}(\sqrt{a_1 P_S}x_1 + \sqrt{a_2 P_S}x_2) + \tilde{h}_{RR}\sqrt{P_R}x_R + z_R, \quad (5)$$

where h_{SR} , \tilde{h}_{RR} are respectively the fading coefficients of the channels from S to R, and from the transmitting to the receiving circuits of R; a_1 and a_2 are power allocation coefficients for each user (NOMA coefficients) with $a_1 > a_2$ and $a_1 + a_2 = 1$; x_1 and x_2 are the two messages for two users D_1 and D_2 , respectively. x_R is the transmitted signals from R; z_R is the Additive White Gaussian Noise (AWGN) with zero-mean and variance of N_R , i.e. $z_R \sim \mathcal{CN}(0, N_R)$.

It is obvious that the self-interference (SI) at the R from the expression (5) can be calculated as

$$\mathbb{E}\{|\tilde{h}_{RR}|^2 P_R\} = \frac{\eta\alpha P}{1 - \alpha} \mathbb{E}\{|\tilde{h}_{RR}|^2 \rho_2\}, \quad (6)$$

where the $\mathbb{E}\{\cdot\}$ is the expectation operator; $\rho_2 = |h_{BR}|^2$. It should be noticed that (6) denotes the SI power before SIC.

Since the relay knows the transmit signal x_R and the estimated SI channel \tilde{h}_{RR} , it can apply the digital methods to subtract the SI from the received signals. We assume that the relay can apply a combination of self-interference cancellation techniques [2, 48, 4, 49], including isolation, propagation domain, digital and analog cancellation. Due to the imperfect hardware and the imperfect estimation of the self-interference channels, after applying all SIC algorithms, the SI cannot be suppressed completely. Obviously, the remaining of SI should have an impact on the system performance. The remaining RSI after SIC, which is denoted by I_R , can be modeled as a complex Gaussian random variable [4, 48, 2, 50, 51] with zero mean and variance $\gamma_{RSI} = \tilde{\Omega} \frac{\eta\alpha P}{1-\alpha}$ ($\tilde{\Omega}$ denotes the SIC capability of the relay node). After SIC, the remaining signal at the R can be expressed as

$$y_R = h_{SR}(\sqrt{a_1 P_S} x_1 + \sqrt{a_2 P_S} x_2) + I_R + z_R. \quad (7)$$

On the other hand, the transmitted signal at the relay node is given by

$$x_R = G y_R, \quad (8)$$

where G is the relaying gain in the AF scheme, which is calculated subject to the fact that the transmit power of the relay node is equal to P_R , that is,

$$\mathbb{E}\{|x_R|^2\} = G^2 \mathbb{E}\{|y_R|^2\} = P_R. \quad (9)$$

When the relay node has perfect knowledge of the fading coefficient h_{SR} , the variable gain corresponding to the fading state is used to improve the system performance. Therefore, we have

$$G \triangleq \sqrt{\frac{P_R}{\rho_3 P_S + \gamma_{RSI} + N_R}} \quad (10)$$

where $\rho_3 = |h_{SR}|^2$ is the square of channel gain amplitude from S to R.

By using the equations (3) and (4), (10) can be rewritten as

$$G \triangleq \sqrt{\frac{\eta\alpha P \rho_2}{\eta\alpha P \rho_1 \rho_3 + (\gamma_{RSI} + N_R)(1-\alpha)}} \quad (11)$$

The received signals at both users D_1 and D_2 are expressed as

$$y_{D_1} = h_{RD_1} x_R + z_1, \quad (12)$$

$$y_{D_2} = h_{RD_2} x_R + z_2, \quad (13)$$

120 where h_{RD_1} and h_{RD_2} are the fading coefficients of the links from R to D_1 and from R to D_2 , respectively; z_1 and z_2 are the AWGNs at the destination nodes, where $z_1 \sim \mathcal{CN}(0, N_1)$ and $z_2 \sim \mathcal{CN}(0, N_2)$.

Now, using (7) and (8), the received signals at D_1 and D_2 are respectively rewritten as

$$y_{D_1} = h_{RD_1} G \left[h_{SR}(\sqrt{a_1 P_S} x_1 + \sqrt{a_2 P_S} x_2) + I_R + z_R \right] + z_1, \quad (14)$$

$$y_{D_2} = h_{RD_2} G \left[h_{SR} (\sqrt{a_1 P_S} x_1 + \sqrt{a_2 P_S} x_2) + I_R + z_R \right] + z_2, \quad (15)$$

In the NOMA systems, the far user (in this paper, this is the user 1, denoted by D_1) decodes its own message in the existence of the interference from the near user (user 2 or D_2 in this paper). The near user D_2 first subtracts the signal from the user D_1 through successive interference cancellation. Then, it decodes its own message. With the assumption of perfect successive interference cancellation, the received signal at the D_2 after removing the interference is given by

$$y_{D_2} = h_{RD_2} G \left[h_{SR} \sqrt{a_2 P_S} x_2 + I_R + z_R \right] + z_2, \quad (16)$$

Therefore, the signal-to-interference-plus-noise ratio SINR at the D_1 through (14) can be calculated as

$$\gamma_{D_1} = \frac{|h_{SR}|^2 |h_{RD_1}|^2 G^2 a_1 P_S}{|h_{SR}|^2 |h_{RD_1}|^2 G^2 a_2 P_S + \gamma_{RSI} + N_R} = \frac{\rho_3 \rho_4 G^2 a_1 P_S}{\rho_3 \rho_4 G^2 a_2 P_S + \gamma_{RSI} + N_R}. \quad (17)$$

where $\rho_4 = |h_{RD_1}|^2$ is the square of channel gain amplitude from R to D_1 .

By substituting (11) into (17), we have:

$$\gamma_{D_1} = \frac{\eta^2 \alpha^2 P^2 a_1 \rho_1 \rho_2 \rho_3 \rho_4}{\eta^2 \alpha^2 P^2 a_2 \rho_1 \rho_2 \rho_3 \rho_4 + \mathcal{A}_1 + \mathcal{B}_1 + \mathcal{C}_1}, \quad (18)$$

where $\mathcal{A}_1 = (1 - \alpha)(\gamma_{RSI} + N_R)\eta\alpha P\rho_2\rho_4$; $\mathcal{B}_1 = (1 - \alpha)N_1\eta\alpha P\rho_1\rho_3$; $\mathcal{C}_1 = (1 - \alpha)^2(\gamma_{RSI} + N_R)N_1$.

Similar to (17), at the user D_2 , the SINR after applying the successive interference cancellation to (15) is given by

$$\gamma_{D_2}^{D_1} = \frac{\eta^2 \alpha^2 P^2 a_1 \rho_1 \rho_2 \rho_3 \rho_5}{\eta^2 \alpha^2 P^2 a_2 \rho_1 \rho_2 \rho_3 \rho_5 + \mathcal{A}_2 + \mathcal{B}_2 + \mathcal{C}_2}, \quad (19)$$

where $\mathcal{A}_2 = (1 - \alpha)(\gamma_{RSI} + N_R)\eta\alpha P\rho_2\rho_5$; $\mathcal{B}_2 = \mathcal{B}_1$; $\mathcal{C}_2 = \mathcal{C}_1$; $\rho_5 = |h_{RD_2}|^2$ is the square of channel gain amplitude from R to D_2 . Due to perfect successive interference cancellation, the SINR at the D_2 after applying successive interference cancellation to (16) can be expressed as

$$\gamma_{D_2} = \frac{\eta^2 \alpha^2 P^2 a_2 \rho_1 \rho_2 \rho_3 \rho_5}{\mathcal{A}_2 + \mathcal{B}_2 + \mathcal{C}_2}. \quad (20)$$

3. Performance Analysis

In this section, we consider the system performance by deriving the outage probability (OP) based on the SINR at the destinations. The system OP is the probability that the instantaneous SINR falls below a pre-defined threshold. We assume that \mathcal{R}_1 and \mathcal{R}_2 (bit/s/Hz) are the minimum required data rates for the users D_1 and D_2 , respectively. In order to maintain the fairness for both users, we set $\mathcal{R}_1 = \mathcal{R}_2 = \mathcal{R}$, thus the OP at the D_1 , which is denoted by $P_{\text{out}}^{D_1}$, can be calculated as

$$P_{\text{out}}^{D_1} = \Pr\{(1 - \alpha) \log_2(1 + \gamma_{D_1}) < \mathcal{R}\} = \Pr\{\gamma_{D_1} < 2^{\frac{\mathcal{R}}{1-\alpha}} - 1\}. \quad (21)$$

Let's denote $x = 2^{\frac{R}{1-\alpha}} - 1$, then (21) can be rewritten as

$$P_{\text{out}}^{\text{D}_1} = \Pr\{\gamma_{\text{D}_1} < x\}. \quad (22)$$

At the D_2 , the outage occurs when it cannot decode successfully either the signal x_1 or its own signal x_2 . Therefore, we have:

$$P_{\text{out}}^{\text{D}_2} = \Pr\{\gamma_{\text{D}_2}^{\text{D}_1} < x, \gamma_{\text{D}_2} < x\} = \Pr\{\min(\gamma_{\text{D}_2}^{\text{D}_1}, \gamma_{\text{D}_2}) < x\}. \quad (23)$$

125 It is also noted that the definition of the OP in (22) and (23) includes the case of low harvested energy at the source and the relay.

Theorem 1. *Under the impact of the RSI and the Rayleigh fading channel, the OPs at the D_1 and D_2 of the FD-NOMA system are determined as*

$$P_{\text{out}}^{\text{D}_1} = \begin{cases} 1 - \sum_{m=1}^M \sum_{n=1}^N \frac{\pi^2 \sqrt{(1-\phi_m^2)(1-\phi_n^2)} X_1 X_2}{4MN\Omega_3\Omega_4 \ln^2 u \ln^2 v} \exp\left(\frac{X_1}{\Omega_3 \ln u} + \frac{X_2}{\Omega_4 \ln v}\right) \sqrt{\frac{4X_3 \ln u \ln v}{X_1 X_2}} K_1\left(\sqrt{\frac{4X_3 \ln u \ln v}{X_1 X_2}}\right) & \text{if } x < \frac{a_1}{a_2} \\ 1 & \text{if } x \geq \frac{a_1}{a_2} \end{cases} \quad (24)$$

$$P_{\text{out}}^{\text{D}_2} = \begin{cases} 1 - \sum_{m=1}^M \sum_{n=1}^N \frac{\pi^2 Y_1 Y_2 \sqrt{(1-\phi_m^2)(1-\phi_n^2)}}{4MN\Omega_3\Omega_5 \ln^2 u \ln^2 v} \exp\left(\frac{Y_1}{\Omega_3 \ln u} + \frac{Y_2}{\Omega_5 \ln v}\right) \sqrt{\frac{4Y_3 \ln u \ln v}{Y_1 Y_2}} K_1\left(\sqrt{\frac{4Y_3 \ln u \ln v}{Y_1 Y_2}}\right) & \text{if } x < \frac{a_1}{a_2} - 1 \\ 1 - \sum_{m=1}^M \sum_{n=1}^N \frac{\pi^2 X_1 X_2 \sqrt{(1-\phi_m^2)(1-\phi_n^2)}}{4MN\Omega_3\Omega_5 \ln^2 u \ln^2 v} \exp\left(\frac{X_1}{\Omega_3 \ln u} + \frac{X_2}{\Omega_5 \ln v}\right) \sqrt{\frac{4X_3 \ln u \ln v}{X_1 X_2}} K_1\left(\sqrt{\frac{4X_3 \ln u \ln v}{X_1 X_2}}\right) & \text{if } \frac{a_1}{a_2} - 1 \leq x < \frac{a_1}{a_2} \\ 1 & \text{if } x \geq \frac{a_1}{a_2} \end{cases} \quad (25)$$

where M and N are the complexity-accuracy trade-off parameters; $\Omega_i = \mathbb{E}(\rho_i)$, $i = 1, 2, \dots, 5$; $K_1(\cdot)$ denotes the first-order modified Bessel function of the second kind, and

$$\begin{aligned} u &= \frac{1}{2} \cos\left(\frac{(2m-1)\pi}{2M}\right) + \frac{1}{2}; \phi_m = \cos\left(\frac{(2m-1)\pi}{2M}\right) \\ v &= \frac{1}{2} \cos\left(\frac{(2n-1)\pi}{2N}\right) + \frac{1}{2}; \phi_n = \cos\left(\frac{(2n-1)\pi}{2N}\right) \\ X_1 &= \frac{(1-\alpha)(\gamma_{\text{RSI}} + N_{\text{R}})x}{\Omega_1 \eta \alpha P(a_1 - a_2 x)}; X_2 = \frac{(1-\alpha)N_1 x}{\Omega_2 \eta \alpha P(a_1 - a_2 x)}; \\ X_3 &= \frac{(1-\alpha)^2 (\gamma_{\text{RSI}} + N_{\text{R}}) N_1 x (a_1 - a_2 x + x)}{\Omega_1 \Omega_2 \eta^2 \alpha^2 P^2 (a_1 - a_2 x)^2}; \\ Y_1 &= \frac{(1-\alpha)(\gamma_{\text{RSI}} + N_{\text{R}})x}{\Omega_1 \eta \alpha P a_2}; Y_2 = \frac{(1-\alpha)N_1 x}{\Omega_2 \eta \alpha P a_2}; \\ Y_3 &= \frac{(1-\alpha)^2 (\gamma_{\text{RSI}} + N_{\text{R}}) N_1 x (a_2 + x)}{\Omega_1 \Omega_2 \eta^2 \alpha^2 P^2 a_2^2}; \end{aligned}$$

Proof: For the $P_{\text{out}}^{\text{D}_1}$, from (22) we have

$$P_{\text{out}}^{\text{D}_1} = \Pr \left\{ \frac{\eta^2 \alpha^2 P^2 a_1 \rho_1 \rho_2 \rho_3 \rho_4}{\eta^2 \alpha^2 P^2 a_2 \rho_1 \rho_2 \rho_3 \rho_4 + \mathcal{A}_1 + \mathcal{B}_1 + \mathcal{C}_1} < x \right\} \quad (26)$$

To derive the $P_{\text{out}}^{\text{D}_1}$ in (24), we apply the equation Eq. (3.324) in [52] with some mathematical calculation. Herein, the channel gains of the Rayleigh fading, ρ_i , $i = 1, 2, \dots, 5$ are determined through the cumulative distribution functions (CDFs), $F_{\rho_i}(x)$, and probability distribution functions (PDFs), $f_{\rho_i}(x)$ as follows:

$$F_{\rho_i}(x) = 1 - \exp\left(-\frac{x}{\Omega_i}\right), x \geq 0, \quad (27)$$

$$f_{\rho_i}(x) = \frac{1}{\Omega_i} \exp\left(-\frac{x}{\Omega_i}\right), x \geq 0. \quad (28)$$

After doing some algebra, (26) becomes (24). The $P_{\text{out}}^{\text{D}_2}$ is obtained by the same method. For details of the proof, see Appendix.

4. Numerical Results

130 In this section, we utilize the theoretical formulas derived in Section 3 to evaluate the system performance of the EH-FD-NOMA system. The Monte-Carlo simulations are also used to verify the analytical results. In this paper, we define the average SNR as the ratio between the transmit power of the PB and the variance of AWGN. For simplicity, we set $N_{\text{R}} = N_1 = N_2$, and hence, $\text{SNR} = P/N_{\text{R}} = P/N_1 = P/N_2$. The remaining simulation parameters to consider are introduced as follows. 135 The energy harvesting efficiency of the nodes in system is $\eta = 0.85$; the power allocation coefficients are set to $a_1 = 0.65$; $a_2 = 0.35$; the average channel gains $\Omega_1 = \Omega_2 = \Omega_3 = \Omega_5 = 1$, $\Omega_4 = 0.7$; the complexity-accuracy trade-off parameters M and N are chosen as $M = N = 10$; the SIC capability $\tilde{\Omega}$ and α are varied to study their impact on the system performance. With these parameters for consideration, we can obtain the similar outage performance of both users.

140 Fig. 3 plots the OP of users D_1 and D_2 versus the average SNR for the proposed EH-FD-NOMA system. Herein, the theoretical curves are plotted by using (24) for D_1 and (25) for D_2 . The data rate to consider for the OP is $\mathcal{R} = 0.3$ bit/s/Hz with the SIC capability $\tilde{\Omega} = -30$ dB. Due to the fact that $\gamma_{\text{RSI}} = \tilde{\Omega} \frac{\eta \alpha P}{1 - \alpha}$, the RSI should increase at high values of SNR. Therefore, the system performance goes to the floor at high SNR regime. It is easy to observe from the Fig. 3 that the outage probabilities of 145 both users decrease when the transmit power at the PB increases. On the other hand, the two users have the same performance and diversity order. In high SNR regime ($\text{SNR} > 35$ dB), the OPs of both users decrease slowly and reach the outage floor due to the RSI. It can be seen from the Fig. 3, the simulation curves exactly match with the corresponding theoretical curves.

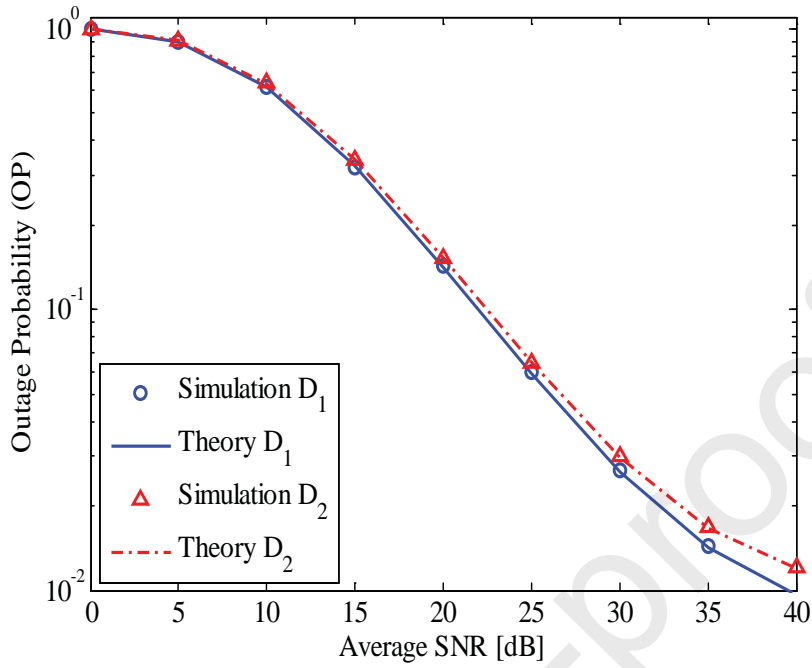


Figure 3: The OP at D_1 and D_2 versus the average SNR with $\alpha = 0.5$, $\tilde{\Omega} = -30$ dB; $\mathcal{R} = 0.3$ bit/s/Hz.

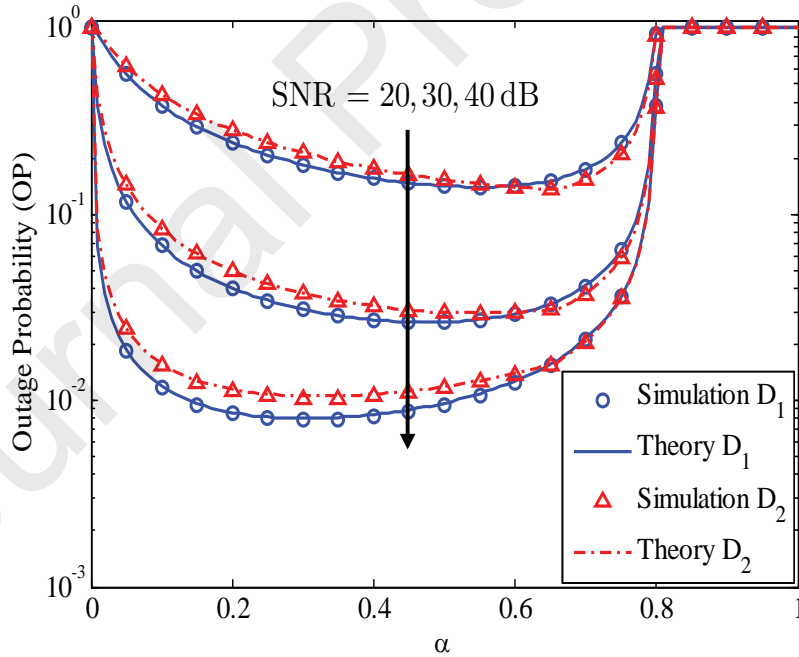


Figure 4: Impact of the time duration EH α to the OP performance of both users with some values of the average SNR.

Fig. 4 shows the OP performance versus the time switching factor for EH, α , for both users with $\mathcal{R} = 0.3$ and $\tilde{\Omega} = -30$ dB. The remaining parameters, i.e. a_1, a_2, \dots , are the same with those in Fig. 3.

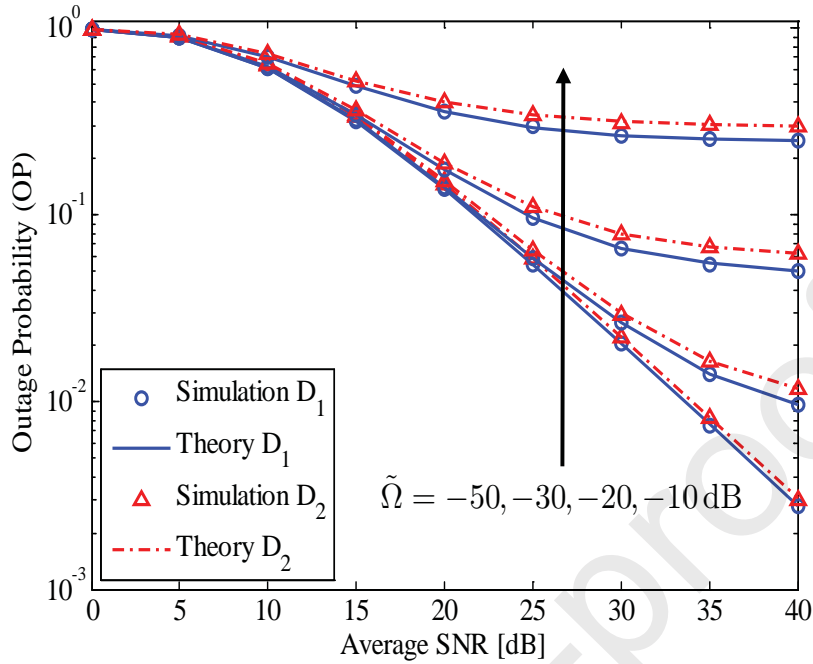


Figure 5: The performance of both users under the impact of SIC capability at the FD node, with $\tilde{\Omega} = -50, -30, -20, -10$ dB.

Fig. 4 shows that when the transmit power at the PB is low, the S and R need more duration for EH. For example, with SNR = 20 dB, the optimal value of α is about 0.6, that means the EH-FD-NOMA system needs more than half of the transmission block for EH. When the transmit power at the PB is higher, for example, SNR = 30 dB, the optimal value of α is reduced, with $\alpha^* = 0.5$. At high SNR (SNR = 40 dB), the optimal value of α is $\alpha^* = 0.3$. Therefore, depending on the transmit power at the PB, the wireless network designers need to choose the suitable duration of EH for this system in practical deployment to improve the system performance. On the other hand, through investigating, the optimal harvesting points of both users are similar as in Fig. 4 when we change the values of the NOMA parameters.

Fig. 5 illustrates the impact of the SIC capability at the FD relay node on the OP performance at both users with $\tilde{\Omega} = -50, -30, -20, -10$ dB, $\alpha = 0.5$, and $\mathcal{R} = 0.3$ bit/s/Hz. As seen from this figure, the SIC capability decides the survival of the system. When the RSI is large, i.e. $\tilde{\Omega} = -10$ dB, the OPs of both users decrease slowly and stay above the outage floor. With the better SIC, i.e. $\tilde{\Omega} = -50$ dB, the OPs decrease faster and fall below the outage floor. Therefore, it is necessary to apply all techniques of SIC in the FD mode to achieve the FD in the realistic scenarios.

Fig. 6 illustrates the delay-sensitive throughput of the proposed EH-FD-NOMA system versus the average SNR for different values of the EH time switching factor, i.e., $\alpha = 0.1, 0.3, 0.5$ and $\mathcal{R} = 0.5$ bit/s/Hz. The throughput values at D_1 and D_2 are defined as $\mathcal{T}_{D_1} = \mathcal{R}(1 - \alpha)(1 - P_{\text{out}}^{D_1})$ and

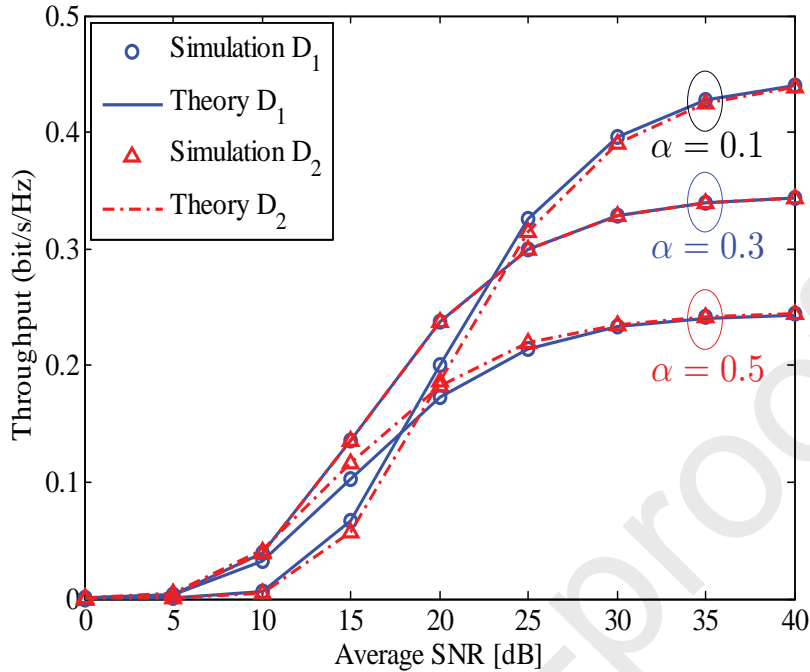


Figure 6: The throughput of the EH-FD-NOMA system versus the average SNR for different values of the time duration energy harvesting, $\alpha = 0.1; 0.3; 0.5$; $\mathcal{R} = 0.5$ bit/s/Hz.

$\mathcal{T}_{D_2} = \mathcal{R}(1 - \alpha)(1 - P_{\text{out}}^{D_2})$, respectively. We can observe that at the low SNR regime (SNR < 20 dB),
 170 the throughput in the case of $\alpha = 0.3$ is the best one among the three cases we consider. However,
 at high SNR regime, i.e. SNR = 40 dB, the case of $\alpha = 0.1$ is the best one. By combining with the
 Fig. 4, it is easy to see that when the transmit power at the PB is sufficiently high, i.e. SNR = 40 dB,
 the selection of $\alpha = 0.1 \rightarrow 0.3$ for our system is the best choice. In fact, with those values of α and
 SNR = 40 dB, the system can attain both performance standards, the outage performance and the
 175 throughput.

5. Conclusion

In this paper, the performance of the EH-FD-NOMA system with amplify-and-forward protocol
 is analyzed. By mathematical analysis, we obtain the closed-form expressions of the OP at two users
 in the presence of the residual self-interference due to the FD mode. The numerical results show that
 180 the performance at the far user can be maintained at the same level with the near user by using
 suitable power allocation coefficients. From the outage and throughput performance at both users,
 the optimal value of the time switching factor for energy harvesting is also figured out. In other words,
 using the PB with high transmit power combined with the SIC for the FD mode can improve both
 the outage performance and the throughput of both users. Furthermore, with the development of

185 antenna and circuit design techniques and the analog and digital signal processing, the operation of
the considered system can be deployed and evaluated in practical scenarios. Therefore, the results in
this paper are important for wireless network designers and researchers in conducting experiments on
the EH-FD-NOMA systems.

Appendix

190 This appendix provides the detailed steps to obtain the outage probability of the proposed EH-
FD-NOMA system over Rayleigh fading channel.

From (26), we have the probability formula as follows:

$$\begin{aligned}
 P_{\text{out}}^{\text{D}_1} &= \Pr \left\{ \frac{\eta^2 \alpha^2 P^2 a_1 \rho_1 \rho_2 \rho_3 \rho_4}{\eta^2 \alpha^2 P^2 a_2 \rho_1 \rho_2 \rho_3 \rho_4 + \mathcal{A}_1 + \mathcal{B}_1 + \mathcal{C}_1} < x \right\} \\
 &= \Pr \left\{ \begin{aligned} &\eta^2 \alpha^2 P^2 \rho_1 \rho_2 \rho_3 \rho_4 (a_1 - a_2 x) < (1 - \alpha)(\gamma_{\text{RSI}} + N_{\text{R}}) x \eta \alpha P \rho_2 \rho_4 \\ &+ (1 - \alpha) N_1 x \eta \alpha P \rho_1 \rho_3 + (1 - \alpha)^2 (\gamma_{\text{RSI}} + N_{\text{R}}) N_1 x \end{aligned} \right\} \quad (29)
 \end{aligned}$$

As shown in second line of (29), when $a_1 - a_2 x \leq 0$, i.e. $x \geq a_1/a_2$, the event in (29) always
occurs. Therefore, $P_{\text{out}}^{\text{D}_1} = 1$ in this case. When $x < a_1/a_2$, the $P_{\text{out}}^{\text{D}_1}$ is calculated as

$$\begin{aligned}
 P_{\text{out}}^{\text{D}_1} &= 1 - \int_0^\infty \int_0^\infty \int_0^\infty \left[1 - F_{\rho_1} \left(\frac{(1 - \alpha)^2 (\gamma_{\text{RSI}} + N_{\text{R}}) N_1 x (a_1 - a_2 x + x)}{\eta^2 \alpha^2 P^2 (a_1 - a_2 x)^2 y \rho_3 \rho_4} + \frac{(1 - \alpha)(\gamma_{\text{RSI}} + N_{\text{R}}) x}{\eta \alpha P (a_1 - a_2 x) \rho_3} \right) \right] \\
 &\times f_{\rho_2} \left(y + \frac{(1 - \alpha) N_1 x}{\eta \alpha P (a_1 - a_2 x) \rho_4} \right) dy f_{\rho_3}(\rho_3) d\rho_3 f_{\rho_4}(\rho_4) d\rho_4 \\
 &= 1 - \int_0^\infty \int_0^\infty \int_0^\infty \exp \left(- \frac{(1 - \alpha)^2 (\gamma_{\text{RSI}} + N_{\text{R}}) N_1 x (a_1 - a_2 x + x)}{\Omega_1 \eta^2 \alpha^2 P^2 (a_1 - a_2 x)^2 y \rho_3 \rho_4} - \frac{(1 - \alpha)(\gamma_{\text{RSI}} + N_{\text{R}}) x}{\Omega_1 \eta \alpha P (a_1 - a_2 x) \rho_3} \right) \\
 &\times \frac{1}{\Omega_2} \exp \left(- \frac{y}{\Omega_2} - \frac{(1 - \alpha) N_1 x}{\Omega_2 \eta \alpha P (a_1 - a_2 x) \rho_4} \right) dy f_{\rho_3}(\rho_3) d\rho_3 f_{\rho_4}(\rho_4) d\rho_4 \\
 P_{\text{out}}^{\text{D}_1} &= 1 - \int_0^\infty \int_0^\infty \exp \left(- \frac{(1 - \alpha)(\gamma_{\text{RSI}} + N_{\text{R}}) x}{\Omega_1 \eta \alpha P (a_1 - a_2 x) \rho_3} - \frac{(1 - \alpha) N_1 x}{\Omega_2 \eta \alpha P (a_1 - a_2 x) \rho_4} \right) \\
 &\times \sqrt{\frac{4(1 - \alpha)^2 (\gamma_{\text{RSI}} + N_{\text{R}}) N_1 x (a_1 - a_2 x + x)}{\Omega_1 \Omega_2 \eta^2 \alpha^2 P^2 (a_1 - a_2 x)^2 \rho_3 \rho_4}} \\
 &\times K_1 \left(\sqrt{\frac{4(1 - \alpha)^2 (\gamma_{\text{RSI}} + N_{\text{R}}) N_1 x (a_1 - a_2 x + x)}{\Omega_1 \Omega_2 \eta^2 \alpha^2 P^2 (a_1 - a_2 x)^2 \rho_3 \rho_4}} \right) f_{\rho_3}(\rho_3) d\rho_3 f_{\rho_4}(\rho_4) d\rho_4 \\
 &= 1 - \int_0^\infty \int_0^\infty \exp \left(- \frac{X_1}{\rho_3} - \frac{X_2}{\rho_4} \right) \sqrt{\frac{4X_3}{\rho_3 \rho_4}} K_1 \left(\sqrt{\frac{4X_3}{\rho_3 \rho_4}} \right) f_{\rho_3}(\rho_3) d\rho_3 f_{\rho_4}(\rho_4) d\rho_4. \quad (30)
 \end{aligned}$$

Herein, we set $\rho_2 = y + \frac{(1 - \alpha) N_1 x}{\eta \alpha P (a_1 - a_2 x) \rho_4}$. As can be seen from (30), it is hard to obtain the closed-
form expression of the $P_{\text{out}}^{\text{D}_1}$ by regular method. To derive the expression from (30), we change the

variable by letting $z = \exp\left(-\frac{X_1}{\rho_3}\right)$. After doing some algebra, we obtain the $P_{\text{out}}^{\text{D}_1}$ by using the Gaussian-Chebyshev quadrature method in [53, 8.4.6] as follows:

$$\begin{aligned} P_{\text{out}}^{\text{D}_1} &= 1 - \int_0^\infty \left[\int_0^1 \frac{X_1}{\Omega_3 \ln^2 z} \exp\left(\frac{X_1}{\Omega_3 \ln z} - \frac{X_2}{\rho_4}\right) \sqrt{\frac{-4X_3 \ln z}{X_1 \rho_4}} K_1\left(\sqrt{\frac{-4X_3 \ln z}{X_1 \rho_4}}\right) dz \right] f_{\rho_4}(\rho_4) d\rho_4 \\ &= 1 - \int_0^\infty \left[\sum_{m=1}^M \frac{\pi X_1 \sqrt{1 - \phi_m^2}}{2M \Omega_3 \ln^2 u} \exp\left(\frac{X_1}{\Omega_3 \ln u} - \frac{X_2}{\rho_4}\right) \sqrt{\frac{-4X_3 \ln u}{X_1 \rho_4}} K_1\left(\sqrt{\frac{-4X_3 \ln u}{X_1 \rho_4}}\right) \right] f_{\rho_4}(\rho_4) d\rho_4. \end{aligned} \quad (31)$$

To resolve the integration in (31), we use the same approach as above. By setting $t = \exp\left(-\frac{X_2}{\rho_4}\right)$, and once again applying the Gaussian-Chebyshev quadrature method, we obtain the $P_{\text{out}}^{\text{D}_1}$ of the considered system as in (24).

For the $P_{\text{out}}^{\text{D}_2}$, similarly to $P_{\text{out}}^{\text{D}_1}$, in the case of $x \geq a_1/a_2$, we have $P_{\text{out}}^{\text{D}_2} = 1$. In the remaining cases, from (23), we derive the probability $P_{\text{out}}^{\text{D}_2}$ as

$$\begin{aligned} P_{\text{out}}^{\text{D}_2} &= \Pr\{\min(\gamma_{\text{D}_2}^{\text{D}_1}, \gamma_{\text{D}_2}) < x\} \\ &= \Pr\left\{ \frac{\eta^2 \alpha^2 P^2 a_1 \rho_1 \rho_2 \rho_3 \rho_5}{\eta^2 \alpha^2 P^2 a_2 \rho_1 \rho_2 \rho_3 \rho_5 + \mathcal{A}_2 + \mathcal{B}_2 + \mathcal{C}_2} < x, \frac{\eta^2 \alpha^2 P^2 a_2 \rho_1 \rho_2 \rho_3 \rho_5}{\mathcal{A}_2 + \mathcal{B}_2 + \mathcal{C}_2} < x \right\} \end{aligned} \quad (32)$$

where the two sub-probabilities of (32) are calculated as

$$\Pr\{\gamma_{\text{D}_2}^{\text{D}_1} < x\} = \Pr\left\{ \begin{array}{l} \rho_5(\eta^2 \alpha^2 P^2 \rho_1 \rho_2 \rho_3 (a_1 - a_2 x) - (1 - \alpha)(\gamma_{\text{RSI}} + N_{\text{R}})x\eta\alpha P\rho_2) \\ < (1 - \alpha)N_1 x\eta\alpha P\rho_1 \rho_3 + (1 - \alpha)^2(\gamma_{\text{RSI}} + N_{\text{R}})N_1 x \end{array} \right\} \quad (33)$$

and

$$\Pr\{\gamma_{\text{D}_2} < x\} = \Pr\left\{ \begin{array}{l} \rho_5(\eta^2 \alpha^2 P^2 \rho_1 \rho_2 \rho_3 a_2 - (1 - \alpha)(\gamma_{\text{RSI}} + N_{\text{R}})x\eta\alpha P\rho_2) \\ < (1 - \alpha)N_1 x\eta\alpha P\rho_1 \rho_3 + (1 - \alpha)^2(\gamma_{\text{RSI}} + N_{\text{R}})N_1 x \end{array} \right\}. \quad (34)$$

From here, we consider the case of $\eta^2 \alpha^2 P^2 \rho_1 \rho_2 \rho_3 (a_1 - a_2 x) - (1 - \alpha)(\gamma_{\text{RSI}} + N_{\text{R}})x\eta\alpha P\rho_2 > \eta^2 \alpha^2 P^2 \rho_1 \rho_2 \rho_3 a_2 - (1 - \alpha)(\gamma_{\text{RSI}} + N_{\text{R}})x\eta\alpha P\rho_2$. It leads to $a_1 - a_2 - a_2 x > 0$, i.e. $x < \frac{a_1}{a_2} - 1$, the conjugation probability in (32) is calculated as $P_{\text{out}}^{\text{D}_2} = \Pr\{\gamma_{\text{D}_2} < x\}$. When the value of x satisfies the condition $\frac{a_1}{a_2} - 1 \leq x < \frac{a_1}{a_2}$, we can obtain the $P_{\text{out}}^{\text{D}_2}$ due to the fact that $P_{\text{out}}^{\text{D}_2} = \Pr\{\gamma_{\text{D}_2}^{\text{D}_1} < x\}$. Therefore, we have three cases for the $P_{\text{out}}^{\text{D}_2}$ of the considered system. On the other hand, the probability in (33) is similar to the probability in (29). Thus, we can be derived the closed-form expression by the same approach as above. For the probability in (34), by setting $\rho_2 = w + \frac{(1-\alpha)N_1 x}{\eta\alpha P a_2 \rho_5}$, we obtain the integral

as follows:

$$\begin{aligned}
\Pr\{\gamma_{D_2} < x\} &= 1 - \int_0^\infty \int_0^\infty \int_0^\infty \left[1 - F_{\rho_1} \left(\frac{(1-\alpha)^2(\gamma_{RSI} + N_R)N_1x(a_2+x)}{\eta^2\alpha^2P^2a_2^2w\rho_3\rho_5} + \frac{(1-\alpha)(\gamma_{RSI} + N_R)x}{\eta\alpha Pa_2\rho_3} \right) \right] \\
&\times f_{\rho_2} \left(w + \frac{(1-\alpha)N_1x}{\eta\alpha Pa_2\rho_5} \right) dw f_{\rho_3}(\rho_3) d\rho_3 f_{\rho_5}(\rho_5) d\rho_5 \\
&= 1 - \int_0^\infty \int_0^\infty \int_0^\infty \exp \left(-\frac{(1-\alpha)^2(\gamma_{RSI} + N_R)N_1x(a_2+x)}{\Omega_1\eta^2\alpha^2P^2a_2^2w\rho_3\rho_5} - \frac{(1-\alpha)(\gamma_{RSI} + N_R)x}{\Omega_1\eta\alpha Pa_2\rho_3} \right) \\
&\times \frac{1}{\Omega_2} \exp \left(-\frac{w}{\Omega_2} - \frac{(1-\alpha)N_1x}{\Omega_2\eta\alpha Pa_2\rho_5} \right) dy f_{\rho_3}(\rho_3) d\rho_3 f_{\rho_5}(\rho_5) d\rho_5 \\
&= 1 - \int_0^\infty \int_0^\infty \exp \left(-\frac{(1-\alpha)(\gamma_{RSI} + N_R)x}{\Omega_1\eta\alpha Pa_2\rho_3} - \frac{(1-\alpha)N_1x}{\Omega_2\eta\alpha Pa_2\rho_5} \right) \sqrt{\frac{4(1-\alpha)^2(\gamma_{RSI} + N_R)N_1x(a_2+x)}{\Omega_1\Omega_2\eta^2\alpha^2P^2a_2^2\rho_3\rho_5}} \\
&\times K_1 \left(\sqrt{\frac{4(1-\alpha)^2(\gamma_{RSI} + N_R)N_1x(a_2+x)}{\Omega_1\Omega_2\eta^2\alpha^2P^2a_2^2\rho_3\rho_5}} \right) f_{\rho_3}(\rho_3) d\rho_3 f_{\rho_5}(\rho_5) d\rho_5 \\
&= 1 - \int_0^\infty \int_0^\infty \exp \left(-\frac{Y_1}{\rho_3} - \frac{Y_2}{\rho_5} \right) \sqrt{\frac{4Y_3}{\rho_3\rho_5}} K_1 \left(\sqrt{\frac{4Y_3}{\rho_3\rho_5}} \right) f_{\rho_3}(\rho_3) d\rho_3 f_{\rho_5}(\rho_5) d\rho_5. \tag{35}
\end{aligned}$$

195 It is obvious that, the expression (35) has the same form as the equation (30), thus it is easy to obtain the closed-form one by the similar method. By applying the the Gaussian-Chebyshev quadrature method [53], the integral in (35) can be resolved. Now, by combining the three cases for the $P_{\text{out}}^{\text{D}_2}$, we obtain the equation (25).

The proof is complete. ■

200 References

- [1] Q. C. Li, H. Niu, A. T. Papathanassiou, G. Wu, 5g network capacity: Key elements and technologies, *IEEE Vehicular Technology Magazine* 9 (1) (2014) 71–78.
- [2] S. Hong, J. Brand, J. I. Choi, M. Jain, J. Mehlman, S. Katti, P. Levis, Applications of self-interference cancellation in 5G and beyond, *IEEE Commun. Mag.* 52 (2) (2014) 114–121. doi: 10.1109/MCOM.2014.6736751.
- 205 [3] F.-L. Luo, C. Zhang, *Signal processing for 5G: algorithms and implementations*, John Wiley & Sons, 2016.
- [4] A. Sabharwal, P. Schniter, D. Guo, D. W. Bliss, S. Rangarajan, R. Wichman, In-band full-duplex wireless: Challenges and opportunities, *IEEE J. Sel. Areas in Commun.* 32 (9) (2014) 1637–1652. doi:10.1109/JSAC.2014.2330193.
- 210

- [5] B. P. Day, A. R. Margetts, D. W. Bliss, P. Schniter, Full-duplex bidirectional mimo: Achievable rates under limited dynamic range, *IEEE Transactions on Signal Processing* 60 (7) (2012) 3702–3713.
- [6] B. C. Nguyen, X. N. Tran, D. T. Tran, Performance analysis of in-band full-duplex amplify-and-forward relay system with direct link, in: 2018 2nd International Conference on Recent Advances in Signal Processing, Telecommunications & Computing (SigTelCom), IEEE, 2018, pp. 192–197.
- [7] B. C. Nguyen, T. M. Hoang, P. T. Tran, Performance analysis of full-duplex decode-and-forward relay system with energy harvesting over nakagami-m fading channels, *AEU-International Journal of Electronics and Communications* 98 (2019) 114–122.
- [8] N. H. Mahmood, G. Berardinelli, F. M. Tavares, P. E. Mogensen, On the potential of full duplex communication in 5g small cell networks., in: *VTC Spring*, 2015, pp. 1–5.
- [9] I. B. Sofi, A. Gupta, A survey on energy efficient 5g green network with a planned multi-tier architecture, *Journal of Network and Computer Applications*.
- [10] S. Chen, B. Ren, Q. Gao, S. Kang, S. Sun, K. Niu, Pattern division multiple access—a novel nonorthogonal multiple access for fifth-generation radio networks, *IEEE Transactions on Vehicular Technology* 66 (4) (2017) 3185–3196.
- [11] Z. Zhang, Z. Ma, M. Xiao, Z. Ding, P. Fan, Full-duplex device-to-device-aided cooperative nonorthogonal multiple access, *IEEE Transactions on Vehicular Technology* 66 (5) (2017) 4467–4471.
- [12] O. Abbasi, A. Ebrahimi, Cooperative noma with full-duplex amplify-and-forward relaying, *Transactions on Emerging Telecommunications Technologies* 29 (7) (2018) e3421.
- [13] Z. Yang, Z. Ding, P. Fan, G. K. Karagiannidis, On the performance of non-orthogonal multiple access systems with partial channel information, *IEEE Transactions on Communications* 64 (2) (2016) 654–667. doi:10.1109/TCOMM.2015.2511078.
- [14] T. Manh Hoang, N. Le Van, B. Nguyen, L. Dung, On the performance of energy harvesting non-orthogonal multiple access relaying system with imperfect channel state information over rayleigh fading channels, *Sensors* 2019 (2019) 1–18. doi:10.3390/s19153327.
- [15] G. Chen, P. Xiao, J. R. Kelly, B. Li, R. Tafazolli, Full-duplex wireless-powered relay in two way cooperative networks, *IEEE Access* 5 (2017) 1548–1558. doi:10.1109/ACCESS.2017.2661378.
- [16] Y. Alsaba, C. Y. Leow, S. K. A. Rahim, Full-duplex cooperative non-orthogonal multiple access with beamforming and energy harvesting, *IEEE Access* 6 (2018) 19726–19738. doi:10.1109/ACCESS.2018.2823723.

- [17] Z. Yan, S. Chen, X. Zhang, H. L. Liu, Outage performance analysis of wireless energy harvesting relay-assisted random underlay cognitive networks, *IEEE Internet of Things Journal* (2018) 1–1doi:10.1109/JIOT.2018.2800716.
- [18] D. H. Chen, Y. C. He, Full-duplex secure communications in cellular networks with downlink wireless power transfer, *IEEE Transactions on Communications* 66 (1) (2018) 265–277. doi:10.1109/TCOMM.2017.2756884.
- [19] Y. Huang, J. Wang, P. Zhang, Q. Wu, Performance analysis of energy harvesting multi-antenna relay networks with different antenna selection schemes, *IEEE Access* 6 (2018) 5654–5665. doi:10.1109/ACCESS.2017.2776934.
- [20] D.-H. Ha, S. T. C. Dong, T. N. Nguyen, T. T. Trang, M. Voznak, Half-duplex energy harvesting relay network over different fading environment: System performance with effect of hardware impairment, *Applied Sciences* 9 (11). doi:10.3390/app9112283.
URL <https://www.mdpi.com/2076-3417/9/11/2283>
- [21] G. Aldawood, H. T. Nguyen, H. Bardaweel, High power density spring-assisted nonlinear electromagnetic vibration energy harvester for low base-accelerations, *Applied Energy* 253 (2019) 113546.
- [22] T. Huguet, M. N. Lallart, A. Badel, Orbit jump in bistable energy harvesters through buckling level modification, *Mechanical Systems and Signal Processing* 128 (2019) 202–215.
- [23] D. Huang, S. Zhou, G. Litak, Analytical analysis of the vibrational tristable energy harvester with a rl resonant circuit, *Nonlinear Dynamics* (2019) 1–15.
- [24] X. Mei, S. Zhou, Z. Yang, T. Kaizuka, K. Nakano, The benefits of an asymmetric tri-stable energy harvester in low-frequency rotational motion, *Applied Physics Express* 12 (5) (2019) 057002.
- [25] S. Beeby, L. Wang, D. Zhu, A. Weddell, G. V Merrett, B. Stark, G. Szarka, B. M Al-Hashimi, A comparison of power output from linear and nonlinear kinetic energy harvesters using real vibration data, *Smart Materials and Structures* 22 (2013) 075022. doi:10.1088/0964-1726/22/7/075022.
- [26] H. Cui, M. Ma, L. Song, B. Jiao, Relay selection for two-way full duplex relay networks with amplify-and-forward protocol, *IEEE Trans. on Wireless Commun.* 13 (7) (2014) 3768–3777. doi:10.1109/TWC.2014.2322607.
- [27] Z. Zhang, Z. Ma, Z. Ding, M. Xiao, G. K. Karagiannidis, Full-duplex two-way and one-way relaying: Average rate, outage probability, and tradeoffs., *IEEE Trans. Wireless Communications* 15 (6) (2016) 3920–3933.

- 275 [28] T. N. Nguyen, D.-T. Do, P. T. Tran, M. Voznak, Time switching for wireless communications with full-duplex relaying in imperfect csi condition, *KSII Transactions on Internet and Information Systems* 10 (9) (2016) 4223–4239. doi:10.3837/tiis.2016.09.011.
- [29] G. Liu, X. Chen, Z. Ding, Z. Ma, F. R. Yu, Hybrid half-duplex/full-duplex cooperative non-orthogonal multiple access with transmit power adaptation, *IEEE Transactions on Wireless Com-*
280 *munications* 17 (1) (2018) 506–519.
- [30] T. M. Hoang, V. Van Son, N. C. Dinh, P. T. Hiep, Optimizing duration of energy harvesting for downlink noma full-duplex over nakagami-m fading channel, *AEU-International Journal of Electronics and Communications*.
- [31] P. Deng, B. Wang, W. Wu, T. Guo, Transmitter design in miso-noma system with wireless-power
285 supply, *IEEE Communications Letters* 22 (4) (2018) 844–847.
- [32] S. Mondal, S. Dhar Roy, S. Kundu, Primary behaviour-based energy harvesting multihop cognitive radio network, *IET Communications* 11 (16) (2017) 2466–2475. doi:10.1049/iet-com.2017.0241.
- [33] M. R. Camana, P. V. Tuan, I. Koo, Optimised power allocation for a power beacon-assisted swipt system with a power-splitting receiver, *International Journal of Electronics* 106 (3) (2019)
290 415–439. doi:10.1080/00207217.2018.1540063.
- [34] N. P. Le, Outage probability analysis in power-beacon assisted energy harvesting cognitive relay wireless networks, *Wireless Communications and Mobile Computing* 2017 (2017) 15. doi:10.1155/2017/2019404.
- 295 [35] V.-D. Phan, T. N. Nguyen, M. Tran, T. T. Trang, M. Voznak, D.-H. Ha, T.-L. Nguyen, Power beacon-assisted energy harvesting in a half-duplex communication network under co-channel interference over a rayleigh fading environment: Energy efficiency and outage probability analysis, *Energies* 12 (13). doi:10.3390/en12132579.
URL <https://www.mdpi.com/1996-1073/12/13/2579>
- 300 [36] X. Lu, P. Wang, D. Niyato, D. I. Kim, Z. Han, Wireless networks with rf energy harvesting: A contemporary survey, *IEEE Communications Surveys Tutorials* 17 (2) (2015) 757–789. doi:10.1109/COMST.2014.2368999.
- [37] C. Zhong, H. A. Suraweera, G. Zheng, I. Krikididis, Z. Zhang, Wireless information and power transfer with full duplex relaying, *IEEE Transactions on Communications* 62 (10) (2014) 3447–
305 3461.

- [38] X. Zhou, R. Zhang, C. K. Ho, Wireless information and power transfer: Architecture design and rate-energy tradeoff, *IEEE Transactions on communications* 61 (11) (2013) 4754–4767.
- [39] Y. S. Cho, J. Kim, W. Y. Yang, C. G. Kang, *MIMO-OFDM wireless communications with MATLAB*, John Wiley & Sons, 2010.
- 310 [40] A. Tulino, A. Lozano, S. Verdú, Mimo capacity with channel state information at the transmitter, in: *Eighth IEEE International Symposium on Spread Spectrum Techniques and Applications-Programme and Book of Abstracts (IEEE Cat. No. 04TH8738)*, IEEE, 2004, pp. 22–26.
- [41] E. Biglieri, R. Calderbank, A. Constantinides, A. Goldsmith, A. Paulraj, H. V. Poor, *MIMO wireless communications*, Cambridge university press, 2007.
- 315 [42] M. Sharma, *Effective channel state information (csi) feedback for mimo systems in wireless broadband communications*, Ph.D. thesis, Queensland University of Technology (2014).
- [43] D.-T. Do, T.-T. T. Nguyen, Impacts of imperfect sic and imperfect hardware in performance analysis on a non-orthogonal multiple access network, *Telecommunication Systems* doi:10.1007/s11235-019-00583-7.
- 320 [44] T. A. Le, H. Y. Kong, Energy harvesting relay-antenna selection in cooperative mimo/noma network over rayleigh fading, *Wireless Networks* doi:10.1007/s11276-019-02051-1.
- [45] M. Liaqat, K. A. Noordin, T. A. Latef, K. Dimiyati, Z. Ding, A. M. Siddiqui, A. Ahmed, T. Younas, Relay selection schemes for cooperative noma (c-noma) with simultaneous wireless information and power transfer (swipt), *Physical Communication* 36 (2019) 100823. doi:<https://doi.org/10.1016/j.phycom.2019.100823>.
- 325 URL <http://www.sciencedirect.com/science/article/pii/S1874490719300783>
- [46] Z. Wang, Z. Peng, Secrecy performance analysis of relay selection in cooperative noma systems, *IEEE Access* 7 (2019) 86274–86287. doi:10.1109/ACCESS.2019.2925380.
- [47] X. Yue, Y. Liu, S. Kang, A. Nallanathan, Z. Ding, Spatially random relay selection for full/half-duplex cooperative noma networks, *IEEE Transactions on Communications* 66 (8) (2018) 3294–3308. doi:10.1109/TCOMM.2018.2809740.
- 330 [48] X. Li, C. Tepedelenlioglu, H. Senol, Channel estimation for residual self-interference in full duplex amplify-and-forward two-way relays, *IEEE Trans. Wireless Commun.* PP (99) (2017) 1–1. doi:10.1109/TWC.2017.2704123.
- 335 [49] K. Yang, H. Cui, L. Song, Y. Li, Efficient full-duplex relaying with joint antenna-relay selection and self-interference suppression, *IEEE Trans. Wireless Commun.* 14 (7) (2015) 3991–4005. doi:10.1109/TWC.2015.2415809.

- [50] X. N. Tran, B. C. Nguyen, D. T. Tran, Outage probability of two-way full-duplex relay system with hardware impairments, in: 2019 3rd International Conference on Recent Advances in Signal Processing, Telecommunications & Computing (SigTelCom), IEEE, 2019, pp. 135–139.
- [51] B. C. Nguyen, X. N. Tran, T. M. Hoang, et al., Performance analysis of full-duplex vehicle-to-vehicle relay system over double-rayleigh fading channels, *Mobile Networks and Applications* (2019) 1–10.
- [52] A. Jeffrey, D. Zwillinger, *Table of integrals, series, and products*, Academic press, 2007.
- [53] F. B. Hildebrand, *Introduction to numerical analysis*, Courier Corporation, 1987.